RSC Advances

ROYAL SOCIETY OF CHEMISTRY

www.rsc.org/advances

RSC Advances

RSC Publishing

ARTICLE

Structural Stability and Bonding Nature of Li-Sn-Carbon Nanocomposite for Anode of Li-Ion Battery: First Principles Approach†

Cite this: DOI: 10.1039/x0xx00000x

Received 00th January 2012,
Accepted 00th January 2012

DOI: 10.1039/x0xx00000x

www.rsc.org/

T. K. Bijoy[a], J. Karthikeyan[b] and P. Murugan[a,b]*

Atomic structural stability and electronic properties of Li_nSn_4-carbon nanotube (CNT) and Li_nSn_4 - graphene nanocomposites were studied by first principles calculations. Results on isolated Li_nSn_4 clusters, with $n = 0 - 10$, revealed that tetrahedron shaped Li_4Sn_4 Zintl cluster is found to be high stable owing to have high symmetry as well as the large highest occupied molecular orbital - lowest unoccupied molecular orbital (HOMO-LUMO) gap. This Li_nSn_4 cluster is weakly interacted with CNT as well as graphene for $n \leq 4$, whereas strong cation-π interaction is observed between them for $n > 4$ which significantly reduces the Li clustering. The interaction between the Sn cluster and CNT or graphene is mediated only through Li ions whose absence destabilizes the Sn-C composite. These results were further confirmed by electronic density of states and band structure calculations. In addition, our calculations on hexagonal assembly of Li_nSn_4/CNT infers that the volume change is minimal during lithiation process and the average intercalation potential is estimated to be maximum of ≈ 0.5 V, which shows its good anodic character.

1. Introduction

Usage of carbonaceous materials in energy storage applications has been increased tremendously after the discovery of several carbon nanostructures, such as, carbon nanotubes (CNT)[1], C_{60} bucky ball[2], graphene[3], and carbon nanofibers[4]. Among various energy storage devices, lithium ion battery (LIB) is widely used in many portable electronic devices[5] due to its high energy density and light weight which keep the attention of scientific as well as industrial researchers. Several attempts have been made to design good materials for its components, essentially electrodes, electrolyte, and separator. In particular, materials for anode have been focused in recent years because the specific capacity could possibly be raised to 4200 mAh/g (theoretical capacity of Si)[6,7]. Though the theoretical capacity of silicon is found to be high, it has severe problem of poor inter particle conductivity due to fracture in particle's structure and this issue can be minimized by controlling particle size[8]. But, graphite is commonly used material for anode due to its low cost and long battery life[9]. However, six carbon atoms together can capture only one Li ion to form stable LiC_6 stoichiometry, which results in low theoretical specific capacity of 372 mAh/g[10], while graphene with few layers carries higher capacity of 700 mAh/g[11]. Compared to this, defect-free single walled CNTs (SWCNTs) have only 400 – 460 mAh/g, but it reaches to 1000 mAh/g for side-wall defective CNTs[12] and this enhancement was reported to be the presence of high porosity and one-dimensionality. However, all these carbon nanostructures have several problems, such as, capacity fading during battery cycle and limitations in the capacity value. Hence, there are many attempts to replace the carbon by some other group IV elements such as Si, Sn, and Pb[13–16]. It is worthy to note that these elements are capable of forming Zintl phase compound with alkali metal atoms which act as cation and Si_n, Sn_n or Pb_n clusters as anion[17, 18]. Compared to carbon, Sn atom has ability to bind with more number of Li ions which results in the formation of $Li_{4.4}Sn$ compound with high theoretical capacity of 994 mAh/g. Howbeit, the drawback in Sn compounds is the problem of colossal volume change during the intercalation process which leads to poor battery life[19].

Concerning the battery life, it is important to find a material exhibiting good capacity with minimal volume change during cycling. It was demonstrated that the composite of nanostructured Sn with multiwalled CNT[20] and carbon nanofibres[21] have been synthesized with greater specific capacity of 889 mAh/g with minimal volume change. Following these works, several reports[22–32] were published in which the Sn-C based composites were shown as a potential candidate for anode of LIB. Though theoretical

[a] *CSIR-Network Institute of Solar Energy (CSIR-NISE), CSIR-Central Electrochemical Research Institute, Karaikudi - 630 006, Tamil Nadu, India.*
[b] *Functional Materials Division, CSIR-Central Electrochemical Research Institute, Karaikudi - 630 006, Tamil Nadu, India.*

† Electronic Supplementary Information (ESI) available: [1] Kohn-Sham energy levels of various clusters, [2] Adsorption energies (E_{ad}) of Li_nSn_4 clusters with various sized armchair CNT, [3] Optimized structure of Li_6Sn_4/(10,10) CNT system, [4] Charge transfer diagram of Li_8Sn_4/(12,6) and Li_8Sn_4/(15,0) systems, [5] Electronic density of states of Li_8Sn_4/(12,6) and Li_8Sn_4/(15,0) systems, [6] Charge transfer diagram of Li_4Sn_4/Gr, Li_6Sn_4/Gr and Li_8Sn_4/Gr systems, [7] Optimized structures of Li_8Sn_4/(9,9) CNT and Li_8Sn_4/double walled CNTs (DWCNT) systems and [8] Li ion intercalation in hexagonal assembly of Li_6Sn_4/(8,8) CNT and Li_8Sn_4/(9,9) CNT systems. See DOI: 10.1039/b000000x/.

understanding on mono-atomic thinned Sn nanowire with SWCNT was reported[31], the structural stability of Li-Sn alloy and its interactions with CNT have not been studied well. Our calculations shed light on atomic structural stability and electronic properties of Li-Sn-CNT composite within density functional theory formalism. We initially studied the growth of Li-Sn alloyed clusters and then, stable clusters were identified and inserted into various sized CNTs for understanding the interaction between them. We also carried out for the deposition of those clusters onto graphene. Our results on Li_nSn_4 clusters with n = 0 - 10 reveal that the Li_4Sn_4 cluster is shown to have ultra high stability with the large highest occupied molecular orbital – lowest unoccupied molecular orbital (HOMO - LUMO) gap as it reaches the Zintl's composition and hence, it interacts weakly with CNT as well as graphene, whereas the clusters with more Li ions (n > 4) bind strongly as the results of significant charge transfer from cluster to CNT, through cation-π interactions. These results were further confirmed by electronic density of states and band structure calculations. In addition, we performed the calculations on assembly of Sn-Li cluster inserted CNTs. It reveals that the volume change is minimal during lithiation process and the average intercalation voltage (AIV) is found to be maximum of ≈ 0.5 V which shows its good anodic character.

2. Computational methods

First principles density functional calculations were performed to understand the structural and electronic properties of Li-Sn cluster inserted SWCNT as implemented in Vienna *Ab-initio* Simulation Package (VASP) [33]. In our calculations, all the atoms were described by projector augmented wave pseudopotential method[34] and electron-electron interaction was correlated by generalized gradient approximations[35]. For Li_nSn_4 clusters, cubic box with a = 15 Å is used to have enough vacuum space between the cluster and its periodic images which will avoid the interaction between them. In the case of isolated CNTs, sufficiently large a and b lattice constants were chosen so that CNT and its periodic images are at least 9 Å apart. Along z-direction, four super cells were constructed with maintaining periodicity. For sampling the Brillouin zone, *Monkhorst-Pack* 1×1×1, 1×1×4, and 2×2×4 ***k***-meshes were used for optimizing the Li-Sn clusters, cluster inserted CNT, and its assembly, respectively. We also repeated the calculations for clusters with denser ***k***-mesh (3×3×3) to ensure its accuracy and negligible energy difference, with maximum of 0.025 eV/atom was observed when compared to ***Γ***-point calculations. Further, 1×1×50 ***k***-mesh was employed for obtaining the density of states (DOS) and band structure of all the systems. All the ions were relaxed self-consistently without considering any symmetry and the iterative relaxation process was repeated until absolute force on each ion was converged to the order of 0.01 eV/Å. The convergence for energy was also set to be 10^{-5} eV throughout our calculations. We repeated all calculations with above mentioned criteria to find the magnetic solution of the system and this solution is favoured for cluster with odd number of electrons. Note that the magnetism in this cluster is completely quenched when it was inserted into SWCNT as significant charge transfer between these two systems is observed from our calculations.

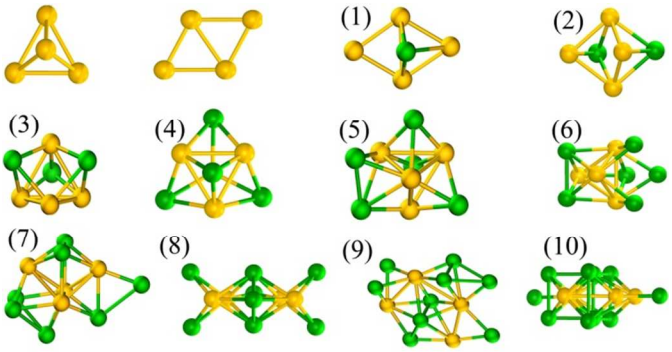

Fig. 1 The ball and stick model of optimized geometry of stable Li_nSn_4 clusters are shown along with Sn_4 tetrahedron and rhombus isomers. n value of cluster is given in parentheses. Yellow and green balls represent Sn and Li atoms, respectively.

3. Results and discussion

We initially considered Sn_4 cluster to understand the lithiation process on it by first principles calculations. Among various isomers, Sn_4 rhombus is found to be stable by 5 meV/atom than its next stable tetrahedron isomer which is in accordance with earlier work[36]. Further, for addition of Li ions on the Sn_4 cluster, both rhombus and tetrahedron isomers (shown in Fig. 1) are considered as this small energy difference between these isomers will be compensated by the Sn-Li alloying energy. Firstly, single Li ion is introduced into various possible sites such as, terminal, edge, and face of them. Our calculations show that Li ion prefers to occupy at their facial site (shown in Fig. 1) rather than edge and terminal sites. The terminal addition is energetically least feasible by 0.22 eV as compared to facial addition, however, the energy of facial and edge Li ion added isomers differ only by 0.01 eV. Hence, further three more Li ions are independently introduced one by one, on the faces and edges of the isomers. Interestingly, it is observed that the optimized geometry of both Li_4Sn_4 isomers is converged into tetrahedron structure. This cluster is commonly known as Zintl cluster and it has Sn_4^{4-} anion[37] which is surrounded by four Li ions acting as cations. By addition of further Li ions on edge (next feasible site) of this cluster, the geometry is transformed to butterfly like structure[38,39] for Li_6Sn_4 and becomes planar one for Li_8Sn_4 cluster (refer Fig. 1). The above discussions indicate that the addition of Li ions strengthens the Sn-Sn bonds by donating the electrons to the Sn-Sn bonding orbitals until n = 4, beyond this, the geometry of cluster is finally converted to planar structure with larger Sn-Sn bonds, which is attributed by the filling of Sn-Sn anti-bonding orbitals (refer Fig. S1, supporting information). In addition to that, clustering of Li ions is also observed for n > 4 case (Table 1). The calculated Sn-Sn, Sn-Li, and Li-Li bond distances were reported in Table 1 and these values are quite consistence with the earlier works[38,39]. Thus, our study reveals that the structural change in pure Sn cluster is unavoidable during Sn-Li alloying process that affects the battery cycle life.

The binding energy per atom (BE) of Li_nSn_4 clusters were calculated for understanding their structural stability from

$$BE = \frac{[4E(Sn) + nE(Li)] - E(Li_nSn_4)}{4 + n} \qquad (1)$$

where $E(Li_nSn_4)$ is the total energy of Li_nSn_4 cluster and $E(Sn)$ and $E(Li)$ are atomic energies of Sn and Li atoms, respectively. The calculated *BE* values are reported in Fig 2. It infers that the BE of Li_nSn_4 clusters decrease with n. Note that all clusters with even n values are found to be more stable than the clusters with odd n as the presence of unpaired electron in HOMO of latter clusters.

Table 1 The average Sn-Sn, Sn-Li, Li-Li, and C-Li bond distances are given for Li-Sn clusters inserted into CNT or deposited on graphene along with E_{ad} and the bader charge per Sn atom (Q_B). Values for isolated clusters are provided in parentheses

System Cluster/CNT	Sn-Sn Å	Sn-Li Å	Li-Li Å	C-Li Å	E_{ad} eV	Q_B e⁻
Sn_4/(8,8)	3.04(2.90)	-	-	-	-2.37	4.00(4.00)
Li_1Sn_4/(8,8)	2.87(2.93)	3.08(2.95)	-	2.44	0.43	4.08(4.22)
Li_2Sn_4/(8,8)	2.87(2.89)	2.93(2.92)	-	2.42	0.41	4.40(4.50)
Li_3Sn_4/(8,8)	2.87(2.95)	3.00(2.86)	-	2.45	0.80	4.44(4.75)
Li_4Sn_4/(8,8)	3.04(3.06)	2.96(2.81)	-	2.58	0.50	4.75(5.00)
Li_6Sn_4/(8,8)	3.02(3.09)	2.95(2.78)	3.25(3.08)	2.5	3.02	4.92(5.50)
Li_8Sn_4/(9,9)	3.05(3.02)	2.90(2.79)	3.12(3.08)	2.50	2.44	5.41(6.00)
Sn_4/Gr	3.05(2.90)	-	-	-	-1.21	4.00(4.00)
Li_2Sn_4/Gr	2.85(2.89)	3.03(2.92)	-	2.53	0.91	4.44(4.50)
Li_4Sn_4/Gr	3.01(3.06)	2.91(2.81)	-	2.65	0.11	4.73(5.00)
Li_6Sn_4/Gr	3.04(3.09)	2.87(2.78)	3.23(3.08)	2.39	1.55	4.98(5.50)
Li_8Sn_4/Gr	3.05(3.02)	2.89(2.79)	2.96(3.08)	2.45	1.02	5.46(6.00)

Among all, Li_4Sn_4 cluster shows the highest stability and large HOMO - LUMO energy gap which is in consistence with earlier report[38]. Such high stability in this cluster is arisen due to its presence of T_d symmetry and the completely filled bonding orbitals (refer Fig. 1, supporting information).

To understand the interaction between cluster and CNT, pristine Sn_4, and Li_nSn_4 clusters were chosen to insert into various sized (m,m) armchair CNTs, where m is the chiral index varying from 7 to 10. The adsorption energy (E_{ad}) is calculated from

$$E_{ad} = E(Li_nSn_4) + E(CNT) - E(Li_nSn_4 + CNT) \qquad (2)$$

where, $E(Li_nSn_4)$, $E(CNT)$, and $E(Li_nSn_4+CNT)$ are total energies of Li_nSn_4 cluster, pristine (m,m) armchair CNT, and Li_nSn_4 inserted CNT, respectively. The E_{ad} values are reported in Table 1 and it shows that this value for pristine Sn_4 cluster loaded CNT is observed to be negative for all the CNTs (eg. -2.37 eV for (8,8) CNT), whereas this value is positive for all lithiated clusters (refer Fig. S2, supporting information). This result clearly indicates that in the absence of Li ions, the Sn cluster will not bind strongly with CNT. Our calculations on preferential radius for inserting cluster into CNT show that (8,8) CNT is apt for clusters with n = 0, 2, 4, and 6, while (9,9) CNT is for Li_8Sn_4 cluster. Then, the calculated E_{ad} values for Sn_4, Li_2Sn_4, Li_4Sn_4, Li_6Sn_4, and Li_8Sn_4 clusters are -2.37, 0.41, 0.52, 3.02, and 2.44 eV, respectively. Thus, our results revealed that the E_{ad} value is drastically increased for n > 4 (after the formation of Zintl cluster). In addition, we have also studied the insertion of clusters into larger sized CNT, in which Li_nSn_4 cluster prefers to interact with one side and 2.19 eV for n = 4 & 6, respectively. Thus, we concluded that the interactions between Sn cluster and carbon nanostructures are mediated only through Li ions, whose absence destabilizes Sn-C composite. of (10,10) CNT's wall (refer Fig. S3, supporting information). As the result of lesser interactions, the E_{ad} values are lowered to 0.32.

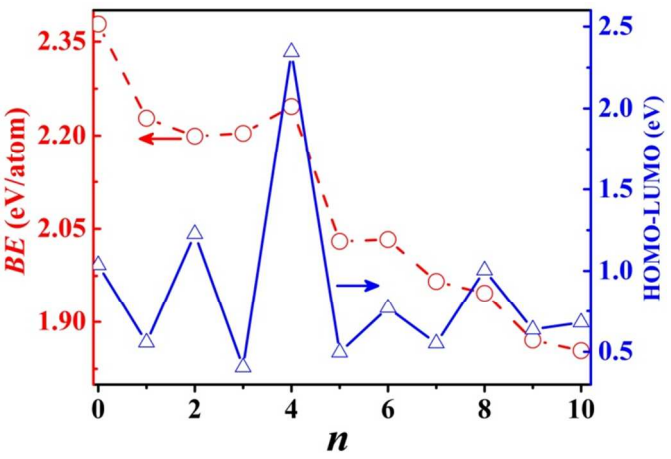

Fig. 2 *BE* and HOMO-LUMO gap of Li_nSn_4 clusters with n = 0 – 10.

To demonstrate the interaction of these clusters with other type CNTs, we have also inserted the Li_8Sn_4 cluster into (12,6) chiral and (15,0) zigzag CNTs which are having almost similar radius of (9,9) armchair CNT (refer Fig. S4, supporting information). The calculated E_{ad} values are 2.02 and 2.56 eV, respectively, which are lesser than that of armchair CNT. The lowering in interaction is due to semiconducting nature of chiral and zigzag CNTs (refer Fig. S5, supporting information). Hence, it is concluded that the size and electronic properties of the cluster and CNTs play vital role in the stability of Sn-Li-CNT composite. These results induced us to study interaction between the planer honeycomb network (graphene) and the lithiated Sn_4 clusters. The calculated E_{ad} of Li_nSn_4/Gr (n = 0, 2, 4, 6 and 8) systems (optimized structure are shown in Fig. S6 of supporting information) follow the same trend with smaller values (refer Table 1), owing to the planar geometry of graphene sheet. As stronger interactions are observed between the CNTs and clusters with n > 4, it is also expected to observe the structural changes in clusters and/or CNTs. For instance, in Li_6Sn_4/(8,8) CNT system, the butterfly like structure of cluster is reverted back to tetrahedron as it transfers excess two electrons to CNT. Note that among Li-Sn clusters, Li_4Sn_4 tetrahedron cluster is highly stable. On the other hand, for Li_8Sn_4/(9,9) CNT case, the geometry cluster is not affected much as all four electrons (compared to Li_4Sn_4 cluster) could not be accepted by CNT. In addition, it is also observed that the Li clusterization is decreased when Li_nSn_4 with n > 4 clusters are inserted inside the CNT. Such reduction in Li dimers/clusters will be beneficial for the electrode system[40].

For example, Li-Li bond distance in Li_6Sn_4 and Li_8Sn_4 clusters are observed to change from 3.08 Å to 3.25 Å and 3.08 Å to 3.12 Å, respectively when these clusters were inserted into CNT (Table 1). Thus, our study shows that if the cluster has more number of Li ions, the shape of the cluster is not changed much when it is inserted inside the CNT. As it is expected, the shape of the CNT is also changed when the Li_8Sn_4 cluster was inserted into (9,9) CNT which is transformed from regular to elliptic cylinder shape, with major to minor axis ratio *(a/b)* of 1.07 and the deformation ($|a - b|$) of 0.82 Å. However, to understand the structural changes in the cluster loaded multiwalled CNTs, we also studied double walled CNT (DWCNT) with inter wall distance of ≈ 3.47 Å, loaded with Li_8Sn_4

cluster (the details are given in Fig. S7, supporting information). Our results show that the *a/b* ratio and $|a-b|$ of inner wall are found to be only 1.02 and 0.26 Å. Hence, we conclude that the outer walls resist the deformation of inner wall during the cluster loading in case of multiwalled CNT.

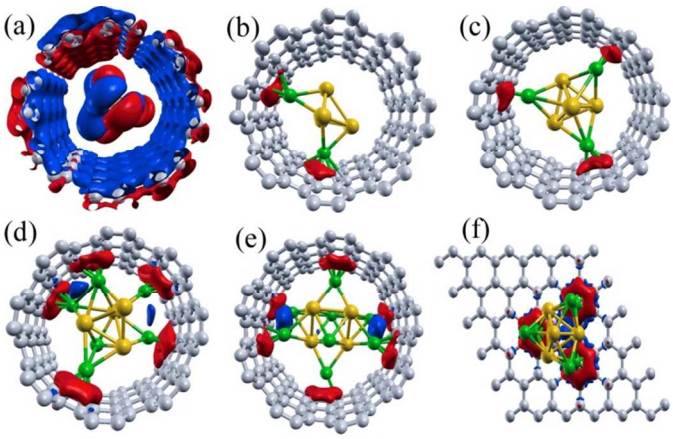

Fig. 3 Red and blue isosurfaces indicate excess and depletion charge in a) Sn_4/(8,8) CNT, b) Li_2Sn_4/(8,8) CNT, c) Li_4Sn_4/(8,8) CNT, d) Li_6Sn_4/(8,8) CNT, e) Li_8Sn_4/(9,9) CNT, and f) Li_6Sn_4/Gr systems. Charge transfer ($\delta\rho$) is calculated from: $\delta\rho = \rho_{cluster} + \rho_{CNT} - \rho_{cluster+CNT}$ where $\rho_{cluster}$, ρ_{CNT} and $\rho_{cluster+CNT}$ are charge densities of cluster, CNT, and cluster loaded CNT, respectively

To understand the nature of interaction qualitatively, the charge transfer between cluster and CNT was plotted for all cases and it is shown in Fig. 3. For lithiated clusters, disc like isosurface is observed between CNT and Li_nSn_4 cluster which explains the charge transfer from Sn-*5p* orbitals to π orbitals of sp^2 hybridized carbon atoms of CNT via Li ions. Similar charge transfer diagram was observed in Fig. S5 (supporting information) for Li ions deposited on the surface of graphene[41] and it is quite resemblance with cation-π interaction which was elaborately discussed[42]. Whereas, no charge transfer between the bare Sn_4 cluster and the CNT is noticed, however, the charge re-population in CNT as well as cluster is observed (refer Fig. 3). Note that though the adsorption energy is found to be small for semiconducting CNT and graphene surface, almost similar charge transfer mechanism was obtained. Overall, this significant charge transfer from Sn-Li clusters to CNT, through cation-π interaction, is attributed to good structural stability of Sn-Li-CNT composites.

Further, to quantify this charge transfer between Li_nSn_4 cluster and CNT, the bader analysis[43] was performed to estimate the valence charge on each atoms and it is reported in Table I. It shows that there is no charge transfer between bare Sn_4 cluster and CNT as valence charge on Sn atoms remains same before and after insertion into CNT which is in consistence with charge transfer plotted in Fig. 3. In case of Li_4Sn_4/(8,8) CNT, totally 1.0 e^- was transferred from Sn-*5p* orbitals to C-*2p* orbitals through Li ions; whereas for Li_6Sn_4 and Li_8Sn_4 clusters, 2.32 and 2.36 e^- have been transferred, respectively (refer Table 1). Hence, the CNT is able to draw the charge from Li_nSn_4 cluster with the maximum limit of ≈ 2.3 e^-. Even though there is nearly equal charge transfer for n = 6 & 8 clusters to CNT, we could observe more number of Li dimers for the latter case which reduces the E_{ad} values. The calculated bader charge for Li_nSn_4/Gr system show that there is no charge transfer from bare Sn_4 cluster to graphene substrate; whereas, comparatively less number of electrons are drawn from the clusters due to less number of C-Li bonds resulted out of planar geometry of the substrate.

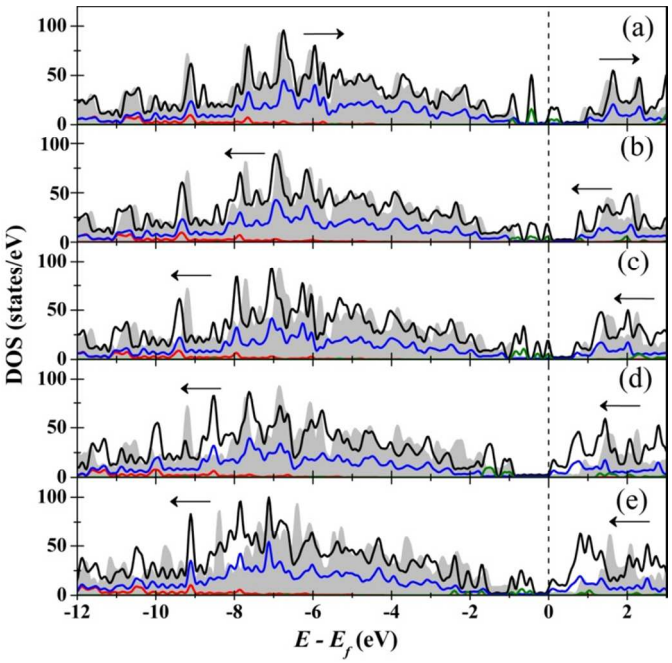

Fig. 4 Total DOS (black solid line) of (a) Sn_4/(8,8) CNT, (b) Li_2Sn_4/(8,8) CNT, (c) Li_4Sn_4/(8,8) CNT, (d) Li_6Sn_4/(8,8) CNT, and (e) Li_8Sn_4/(9,9) CNT systems. C-*2s*, C-*2p*, and Sn-*5p* states are represented by red, blue, and green solid lines. Total DOS of bare CNT is given in background and direction of arrows depicts the shifting of energy levels, reference to bare CNT.

To explore the electronic properties of Li_nSn_4/CNT system, the density of states (DOS) for all systems are deduced and reported in Fig. 4. It is observed in all cases that the sp^2 hybridized states of carbon atoms are distributed in the energy range from -12 eV to -9 eV, whereas the C-*2p* bands are spreading over the entire range (-12 eV to -1 eV). It is also noticed that the states of Sn-*5s* (not shown in Fig. 4) and *5p* states are pronounced as narrow peaks because the electrons in these states are well localized due to ionic character of Sn-Li bond. The DOS of bare Sn_4/(8,8) CNT shows that the occupied states are shifted (as indicated by arrows) slightly towards Fermi energy (E_f) when compared to pristine CNT which again manifests the poor stability of Sn-CNT composite in the absence of lithium. On the other hand, the total occupied DOS of Li_nSn_4/CNT systems with n =2, 4, 6, and 8 are shifted away from E_f by 0.07, 0.20, 0.78 and 0.73 eV, respectively, which give the obvious reason for good stability of Sn-Li-CNT composites.

The band structure calculations were performed for cluster inserted CNT systems to understand the electrons occupancy in Sn-*5p* levels and filling of C-*2p* bands. In Sn_4/(8,8) CNT system, two bands originated from C-$2p_z$ orbitals are crossing the E_f and forming *Dirac* cone like feature at E_f+0.5 eV. The singly and triply degenerated localized Sn-*5p* states are completely occupied and observed at E_f -0.5 eV and E_f , respectively, whereas two unoccupied bonding Sn-*5p* states are lied closer to E_f +0.5 eV. These empty states are getting filled when the bare Sn_4 cluster is lithiated. For instance, five Sn-*5p* states are occupied for Li_2Sn_4/(8,8) CNT system

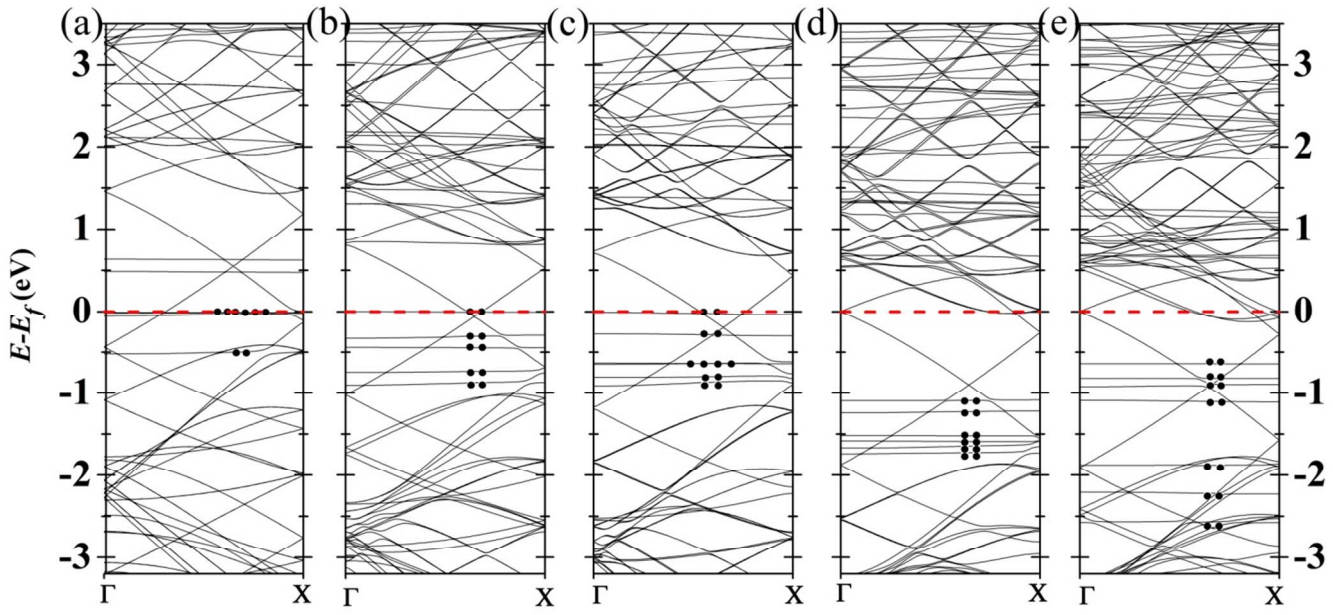

Fig. 5 Electronic band structure of a) Sn_4/(8,8) CNT, b) Li_2Sn_4/(8,8) CNT, c) Li_4Sn_4/(8,8) CNT, d) Li_6Sn_4/(8,8) CNT, and e) Li_8Sn_4/(9,9) CNT systems. Solid dots represent electron occupancies in Sn-*5p* levels.

and the C-*2p* bands are further filled, but not completely, due to the limited charge transfer from the Li ions. On the other hand, the Li_4Sn_4/(8,8) CNT and Li_6Sn_4/(8,8) CNT systems have same number of occupied Sn-*5p* states, because two electrons in the antibonding states of latter system is transferred to fill the C-*2p* bands completely which was partially filled in the former case. Because of this charge transfer, the Li_6Sn_4 cluster changes both geometry and electronic structure as similar to that of Li_4Sn_4 Zintl cluster owing to have large HOMO-LUMO gap. Note that the C-*2p* bands are completely filled in this case. Hence, Li_8Sn_4 cluster could not able to transfer all four excess electrons (compared to Li_4Sn_4 cluster) to CNT's C-*2p* bands; instead only two electrons are transferred as similar to Li_6Sn_4 case. As the result of this less charge transfer, the cluster is not able to attain stable state. Moreover, in this case, the Sn-*5p* level of cluster is well separated which indicates that the cluster reduces its symmetry due to a planar structure. Hence we conclude that the CNT is not able to draw all the electrons from the Li_nSn_4 with (n > 6) cluster that is electronically limited by the completely filled C-*2p* bands of CNT.

The results of cluster filled CNTs motivated us to form a hexagonal assembly to study the Li-ion intercalation properties (refer Fig. S7, supporting information). Generally, Li ions prefer to occupy at the voids of assembly. Here, Li ions are added one by one in well separated sites to reduce the columbic repulsion between them. The average intercalation voltage (AIV)[44] is calculated using Nernst equation,

$$AIV = -\frac{[E(Li_{x2}@Li_nSn_4) - E(Li_{x1}@Li_nSn_4) - (x1 - x2)E(Li)]}{(x2 - x1)F} \quad (3)$$

where $E(Li_{x1}@Li_nSn_4)$ and $E(Li_{x2}@Li_nSn_4)$ are total energies of x_1 and x_2 Li ions intercalated in Li_nSn_4 cluster inserted into (m,m) CNT, respectively. E(Li) and F are total energy per atom of Li-metal and Faraday constant (=1). Calculated *AIV* for Sn_4/(8,8) CNT, Li_2Sn_4/(8,8) CNT, Li_4Sn_4/(8,8) CNT, Li_6Sn_4/(8,8) CNT, and Li_8Sn_4/(9,9) CNT systems are ≈ 0.49, 0.22, 0.19, 0.07, and -0.11 V, respectively. Thus, our results show that Li-Sn-CNT composite is potentially used for anode of Li-ion battery. Moreover, the volume change during lithiation is observed to be minimum (only 0.33%).

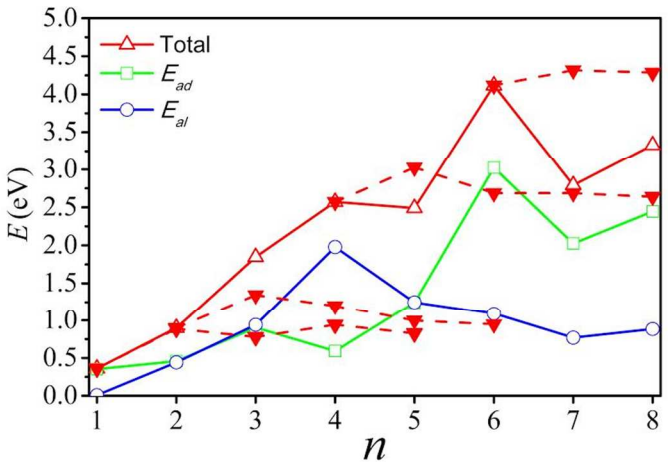

Fig. 6 The composition energy of Li-Sn-CNT (total) versus number of Li ions (n) is shown along with Sn-Li alloying energy (E_{al}), adsorption energy (E_{ad}) and intercalation energy (dotted line).

Based on the energetics obtained from first principles calculations, it is found that the lithiation of anode during first cycle of charging happens in three stages. Firstly, the Li ion prefers to alloy with Sn to form the Zintl cluster; secondly, it forms composite *via* cation-π interaction and thirdly, it intercalates in the pores of CNT assembly. Now, the composite formation energy of Li-Sn-CNT system is defined as $E_c = E_{al} + E_{ad}$. First term, E_{al} is estimated from:

$$E_{al} = E(Sn_4) + n\,\mu(Li) - E(Li_nSn_4) \quad (4)$$

where μ(Li) is chemical potential of Li metal, $E(Sn_4)$ and $E(Li_nSn_4)$ are total energy of Sn_4 and Li_nSn_4 clusters, respectively. Here, we

used the chemical potential of Li to calculate E_{al} as alloying occurs between Sn_4 cluster and Li metal. The calculated E_c values are shown in Fig 6 and it infers that until n = 4, the alloying process dominates, whereas for n > 4, E_{ad} is found to be larger than E_{al}. Hence, the Sn-Li-Carbon composite is formed in this region. To find the feasibility of intercalation process, we also plotted the intercalation energy (shown as dotted lines in Fig. 6) of Li_nSn_4 (n = 0, 2, 4, 6) clusters by considering the respective E_c as origin. From this, it is clearly observed that the value of E_c is always higher than that of intercalation energy until n = 6; so, the intercalation in the pores of CNTs assembly dominates only after this limit. Since the E_{al} and E_{ad} values are comparatively larger than the energetics of intercalation process, it is very difficult to gain back all the Li ions from the composites for n ≤ 6. Thus, the capacity of the material is expected to fade as observed in experiment[20]. However, constant capacity will be retained afterwards as E_c is saturated beyond n = 6.

4. Conclusions

By employing the first principles density functional calculations, the structural stability and electronic properties of Li_nSn_4 (n = 0 - 10) clusters and these clusters loaded CNTs were studied. Among clusters, Li_4Sn_4 Zintl cluster was found to be more stable as it has tetrahedral symmetry and the large HOMO-LUMO gap. Our calculations revealed that the insertion of non-lithiated Sn_4 cluster into CNT was shown to be unstable due to negative adsorption energy that is reflected as charge polarization on CNT as well as cluster. On the other hand, lithiated Sn cluster is preferred to insert into CNT as significant charge transfer from Sn-*5p* states to C-*2p* states through Li ions, by cation-π interaction which was confirmed by electronic density of states and band structure calculations. Similar study was repeated for deposition of cluster onto graphene and results almost reproduced with smaller effect owing to its planar nature. As the result of strong interaction between CNT and lithiated cluster, it reduces Li dimmers as well as, in certain case, the geometry of SWCNT is deformed from regular circular to elliptic cylinder shape. We also demonstrated that this deformation is controlled by introducing MWCNT. In addition, we also show that this composite may be used for anode of Li-ion battery as maximum intercalation potential is observed to be ≈ 0.5 V.

Acknowledgements

We acknowledge T. Prem Kumar for initiating this work. This work is supported by CSIR, India through TAPSUN (NWP-56) project. We also extend it for CSIR - CECRI, CSIR - NCL and CSIR - CMMACS for sharing their HPC facilities.

Notes and references

1 M. S. Dresselhaus, G. Dresselhaus and P.C. Eklund, *Science of Fullerenes and Carbon Nanotubes*, Academic press, 1996.
2 (a) P. Ball, *Nature*, 1991, **354(6348)**, 18; (b) H.P. Schultz, *J. Org. Chem.* 1965, **30**, 1361.
3 A. K. Geim and K. S. Novoselov, *Nat. Mater.,* 2007, **6**, 183.
4 M. Endo and H.W. Kroto, *J. Phys. Chem.,* 1992, **96**, 6941.
5 J. B. Goodenough and K. -S. Park, *J. Am. Chem. Soc*., 2013, **135**, 1167.
6 C. K. Chan, R. Ruffo, S. S. Hong, R. A. Huggins and Y. Cui, *J. Power Sources,* 2009, **189**, 34.
7 H. Wu, G. Zheng, N. Liu, T. J. Carney, Y. Yang and Y. Cui, *Nano Lett.,* 2012, **12**, 904.
8 Z. Ma, T. Li, Y. L. Huang, J. Liu, Y. Zhou and D. Xueb, *RSC Adv.,* 2013, **3**, 7398.
9 C. de las Casas and W. Li, *J. Power Sources*, 2012, **208**, 74.
10 K. -L. Lee, J. Y. Jung, S. -W. Lee, H. -S. Moon and J. -W. Park, *J. Power Sources*, 2004, **129**, 270.
11 E. Yo, J. Kim, E. Hosono, H. Zhou, T. Kudu and I. Honma, *Nano Lett.,* 2008, **8**, 2277.
12 B. J. Landi, M. J. Ganter, C. D. Cress, R. A. DiLeo and R. P. Raffaelle, *Energy Environ. Sci.,* 2009, **2**, 638.
13 C. -M. Park, J. -H. Kim, H. Kim and H. -J. Sohn, *Chem. Soc. Rev.,* 2010, **39**, 3115.
14 T. Zhang, L. J. Fu, J. Gao, Y. P. Wu, R. Holze and H. Q. Wu, *J. Power Sources*, 2007, **174**, 770.
15 X. Wang, Z. Wen, Y. Liu and X. Wu, *Elecrochem. Acta*, 2009, **54**, 4662.
16 P. Meduri, C. Pendyala, V. Kumar, G. U. Sumanasekara and M. K. Sunkara, *Nano lett.,* 2009, **9**, 612.
17 S. Scharfe, F. Kraus, S. Stegmaier, A. Schier and T. F. Fassler, *Angew. Chem. Int. Ed.* , 2011, **50**, 3630.
18 R.Winter, O. Leichtweib , C. Biermann, M. -L. Saboungi, R. L. McGreevy and W. S. Howells, *J. Non-Crystalline Solids,* 1996, **66**, 205.
19 M. Winter and J. O. Besenhard, *Electrochim. Acta,* 1999, **45**, 31.
20 T. P. Kumar, R. Ramesh, Y. Y. Lin and G. T. -K. Fey, *Electrochem. Commun.,* 2004, **6**, 520.
21 Y. Yu, L. Gu, C.Wang, A. Dhanabalan and P. A. van Aken and J. Maier, *Angew. Chem. Int. Ed.,* 2009, **48**, 6485.
22 G. Derrien, J. Hassoun, S. Panero and B. Scrosati, *Adv. Mater.,* 2007, **19**, 2336.
23 J. Qin, C. He, Z. Wang, C. Shi and E. -Z. Liu, *ACS Nano,* 2014, **8**, 1728.
24 Y. Sun, Q.Wu and G. Shi, *Energy and Environ. Sci.,* 2011, **4**, 1113.
25 G. Wang, B. Wang, X. Wang, J. Park, S. Dou, H. Ahn and K. Kim, *J. Mater. Chem.,* 2009, **19**, 8378.
26 M. Noh, Y. Kwon, H. Lee, J. Cho, Y. Kim and M. G. Kim, *Chem. Mater.,* 2005, **17**, 1926.
27 Y. Wang, M. Wu, Z. Jiao and J. Y. Lee, *Chem. Mater.,* 2009, **21**, 3210.
28 Y. Yu, L. Gu, C. Zhu, P. A. van Aken and J. Maier, *J. Am. Chem. Soc.,* 2009, **131**, 15984.
29 Z. Wen, S. Cui, H. Kim, S. Mao, K. Yu, G. Lu, H. Pu, O. Mao and J. Chen, *J. Mater. Chem.*, 2012, **22**, 3300.
30 Y. Xu, J. Guo and C. Wang, *J. Mater. Chem*., 2012, **22**, 9562.
31 M. -F. Ng, J. Zheng and P. Wu, *J. Phys. Chem. C*, 2010, **114**, 8542.
32 W. Jiang, W. Zeng, Z. Ma, Y. Pan, J. Lin, and C. Lu, *RSC. Adv.,* 2014, **4**, 41281.
33 G. Kresse and D. Joubert, *Phys. Rev. B,* 1999, **59**, 1758.
34 P. E. Blochl, *Phys. Rev. B*, 1994, **50**, 17953.
35 J. P. Perdew, J. A. Chevary, S. H. Vosko, K. A. Jackson, M. R. Pederson, D. J. Singh and C. Fiolhais, *Phys. Rev. B*, 1992, **46**, 6671.
36 R. Pushpa, S. Narasimhan and U. Waghmare, *J. Chem. Phys.,* 2004, **121**, 5211.
37 W. J. Zheng, O. C. Thomas, J. M. Nilles, K. H. Bowen, A. C. Reber and S. N. Khanna, *J. Chem. Phys.,* 2011, **134**, 224307.
38 B.Wang, M. J. Stott and J. A. Alonso, *Phys. Rev. B*, 2002, **65**, 045410.
39 M. S. Lee, D. G. Kanhere and K. Joshi, *Phy. Rev. A*, 2005, **72**, 015201.
40 X. Fan, W. T. Zheng, J. -L. Kuo and D. J. Singh, *App. Mater. Interfaces*, 2013, **5**, 7793.
41 K. Rana, G. K. Dogu, H. S. Sen, C. Boothroyd, O. Gulseren and E. Bengu, *J. Phys. Chem. C*, 2012, **116**, 11364.
42 A. S. Mahadevi and G. N. Sastry, *Chem. Rev.,* 2012, **113**, 2100.

43 G. Henkelman, A. Arnaldsson and H. Jonsson, *Comput. Mater. Sci.,* 2006, **36**, 254.
44 K. Persson, Y. Hinuma, Y. S. Meng, A. V. der Ven and G. Ceder, *Phys. Rev. B,* 2010, **82**, 125416.

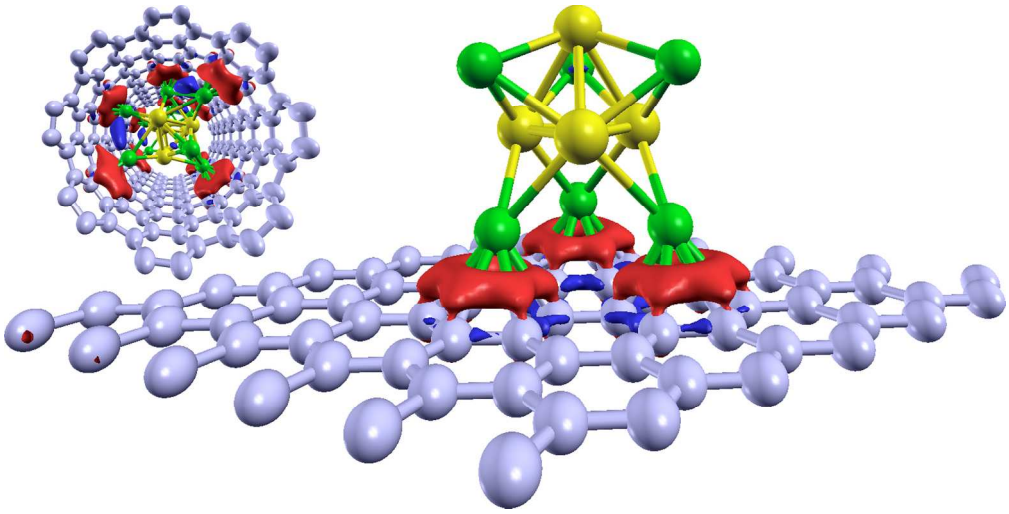

180x90mm (300 x 300 DPI)